Towards a realistic explosion landscape for binary population synthesis

Rachel A. Patton[1]★ and Tuguldur Sukhbold [1,2]†

[1]*Department of Astronomy, The Ohio State University, 140 West 18th Ave, Columbus, OH 43210, USA*
[2]*Center for Cosmology and AstroParticle Physics, The Ohio State University, 191 West Woodruff Avenue, Columbus, OH 43210, USA*

ABSTRACT

A crucial ingredient in population synthesis studies involving massive stars is the determination of whether they explode or implode in the end. While the final fate of a massive star is sensitive to its core structure at the onset of collapse, the existing binary population synthesis studies do not reach core collapse. Instead, they employ simple prescriptions to infer their final fates without knowing the pre-supernova core structure. We explore a potential solution to this problem by treating the carbon-oxygen (CO) core independently from the rest of the star. Using the implicit hydrodynamics code KEPLER, we have computed an extensive grid of 3496 CO-core models from a diverse range of initial conditions, each evolved from carbon ignition until core collapse. The final core structure, and thus the explodability, varies non-monotonically and depends sensitively on both the mass and initial composition of the CO core. Although bare CO cores are not perfect substitutes for cores embedded in massive stars, our models compare well both with MESA and full hydrogenic and helium star calculations. Our results can be used to infer the pre-supernova core structures from population synthesis estimates of CO-core properties, thus to determine the final outcomes based on the results of modern neutrino-driven explosion simulations. A sample application is presented for a population of Type-IIb supernova progenitors.

Key words: stars: evolution – stars: massive – supernovae: general.

1 INTRODUCTION

Massive stars tend to live in binary systems, with 50–70 per cent, of O-type stars exchanging mass with their companion and a third of mass-transfer binaries merging over the lifetime of the primary star (e.g. Sana et al. 2012, 2013, and references therein). Binary interactions can drastically alter the evolution of a massive star, its ultimate demise, properties of the transient, and the compact remnant it produces. To understand how true populations of massive stars evolve and die, we must consider binary interactions.

There is a rich literature of binary population synthesis (BPS) studies aimed at doing just that. Some recent examples include studies of the compact object mass distribution (e.g. Spera, Mapelli & Bressan 2015), of the progenitors of long-duration gamma-ray bursts (Chrimes, Stanway & Eldridge 2020), binary merger and mass transfer rates (de Mink et al. 2014), compact object mergers (Belczynski et al. 2016; Stevenson, Berry & Mandel 2017b; Langer et al. 2020), supernova rates (e.g. Zapartas et al. 2017; Sravan, Marchant & Kalogera 2019; Zapartas et al. 2019), and the ejection of binary companions (e.g. Renzo et al. 2019; Evans, Renzo & Rossi 2020). These types of investigations play a critical role in interpreting various modern observations, including those from transient surveys, gravitational wave radiation, and astrometry.

Carefully following the complete evolution of both stars in a binary system, from zero-age main sequence (ZAMS) until core

collapse, including their often-complicated interactions, can be a challenging problem for a single binary system, let alone for an entire population. The BPS community employs various innovative ways to circumvent these difficulties, for example, by not evolving the stars until core collapse, and often by not directly simulating their evolution. The so-called rapid BPS studies use a semi-analytical approach to approximate stellar evolution through the asymptotic giant branch based on fits from Hurley, Pols & Tout (2000), Hurley, Tout & Pols (2002), modified to include binary interactions (see e.g. Belczynski, Kalogera & Bulik 2002a; Belczynski, Bulik & Kluźniak 2002b; De Donder & Vanbeveren 2004; Izzard et al. 2004, 2006, 2009; Stevenson et al. 2017a; Giacobbo & Mapelli 2018; Giacobbo, Mapelli & Spera 2018; Breivik et al. 2019). Some groups actively follow the evolution using stellar evolution codes, but they cut-off at carbon or neon ignition to avoid and the advanced stages of evolution (e.g. Eldridge, Izzard & Tout 2008; Siess et al. 2013; Eldridge et al. 2017). Still others interpolate over tables of single star models, modified with binary interaction prescriptions (Spera et al. 2015; Spera & Mapelli 2017; Kruckow et al. 2018; Spera et al. 2019).

Failing to reach core collapse is a common problem for BPS studies, especially those investigating the final demise of binary massive stars. It has been known for some time that not only the properties of the explosion, but the very fate of the star, whether it explodes or not, is closely tied to the pre-supernova structure of the core of the massive star (Burrows, Hayes & Fryxell 1995; Fryer 1999; O'Connor & Ott 2011; Pejcha & Thompson 2015; Ertl et al. 2016). This final structure, moments before collapse, is largely set by the advanced stages of evolution in the core, from

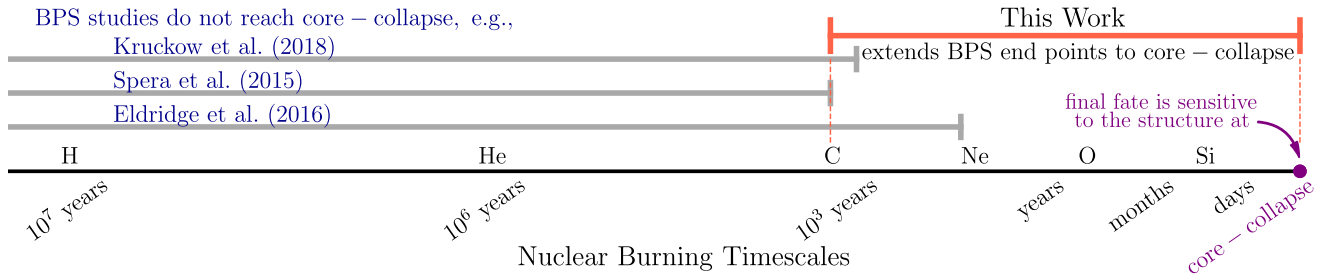★ E-mail: patton.502@osu.edu
† NASA Hubble Fellow.

Figure 1. A comparison of the evolutionary stages covered by BPS studies and our bare CO-core models. Although the final fates and the properties of collapse are sensitive to the core structure at the time of collapse (highlighted in purple), BPS studies follow stellar evolution only until carbon or neon ignition in the centre (grey bars). Falling short of core collapse, BPS studies infer the final outcomes through simple prescriptions that are based on the stellar mass and the embedded He- or CO-core masses, which do not cleanly correlate with the final core structure. This work aims to bridge the evolutionary gap, shown in red, between the cut-off of BPS studies and core collapse, and allows mapping of final outcomes determined from the pre-supernova core structure back to core properties at carbon ignition.

carbon ignition until the iron-core collapse (e.g. Woosley, Heger & Weaver 2002; Sukhbold & Woosley 2014; Sukhbold et al. 2016; Sukhbold & Adams 2020). However, BPS studies never follow this crucial and final part of the star's life taking place inside the carbon–oxygen (CO) core during the final few thousand years (see Fig. 1). Evolution typically stops at carbon ignition or, at the latest, neon ignition. Doing this avoids the extra computational expense and the associated uncertainties of late-stage evolution until the formation and collapse of the iron core. Nevertheless, nearly all BPS studies then must indirectly infer the final fates and the properties of the transients and remnants *without* calculating the pre-supernova core structure.

Instead, BPS calculations (and many studies of single star populations as well, e.g. Eldridge & Tout 2004) attempt to determine which stars die in a supernova, as well as the masses of their compact remnants, by using the ZAMS mass, the mass of the star at the evolutionary cut-off, and the embedded He- or CO-core masses individually or in some combination. For instance, Hurley et al. (2000) introduced a method to infer the remnant types and their respective masses largely from the CO-core mass, while Eldridge & Stanway (2016) used the prescription by Eldridge & Tout (2004) to determine the type of remnant based on the He-core mass, and applied simple energy constraints to estimate their masses. One commonly employed approach, especially in rapid BPS studies (see e.g. Vigna-Gómez et al. 2018), is the 'delayed' prescription by Fryer et al. (2012), which uses the final stellar mass inferred for the pre-supernova stage in combination with the embedded CO-core mass. More recently, Zapartas et al. (2019) assumed all stars that form a core more massive than the one embedded in a star with an initial mass of 20 $M_\odot$ would not produce a supernova. These methods are not uniform and the results can be difficult to interpret, especially when final fates are not based on actual core structure.

Using ZAMS mass, final stellar mass, or CO-core mass to infer the final properties is also generally too simplistic. For instance, it is well known that the evolution of the CO core not only depends on its mass but also depends strongly on its initial composition. Two stars that form CO cores of the same mass but with different initial core compositions can end up with very different final structures, and thus final fates. Moreover, these methods do not capture the non-monotonic variation of the pre-supernova core structure with mass that emerges from the interplay between convective burning episodes of carbon and oxygen (Sukhbold & Woosley 2014; Sukhbold, Woosley & Heger 2018; Sukhbold & Adams 2020). One of the main

implications is that there is no single threshold mass that cleanly delineates explosion versus implosion, that is, no CO-core or ZAMS mass where all lighter stars are likely to die in a supernova and all heavier stars likely to implode. Calibrated neutrino-driven explosion surveys of single stars (e.g. Pejcha & Thompson 2015; Sukhbold et al. 2016) and of stripped cores in close binary systems (Ertl et al. 2020) have demonstrated that the non-monotonically varying final core structures significantly affect the resulting remnant masses, nucleosynthesis, and light curves.

We explore one potential solution to this problem by carrying out the evolution of the stellar core starting from the point where BPS studies typically stop all the way until they experience core collapse. Due to extremely short nuclear-burning timescales, we can approximately treat the evolution of the CO core independently from the rest of the star. Because of its fast pace, the 'accelerated' evolution of the CO core is also fairly immune to major uncertainties of stellar evolution, such as mass loss and rotation. Here, we create a large suite of constant mass CO cores covering a wide range of possible combinations of starting mass and composition, each evolved from the ignition of carbon in the centre until the pre-supernova stage. In reality, of course, the CO-core mass is not truly constant, the 'frozen-envelope' approximation is not entirely valid, and certain rare types of binary interactions may directly alter the evolution of the core. Nevertheless, this approach provides a simple way to connect the endpoints of most stellar models in BPS studies to specific pre-supernova core structures.

Just knowing the final core structure for each star in a BPS simulation does not automatically produce more accurate results for final fates, but it does open the door to explore more physics-based methods. There have been a number of studies in the past decade, with varying complexity, attempting to connect the pre-supernova core structure with the final fate of the star and the properties of the supernova explosion. The simplest, and perhaps the most commonly employed, approach is the compactness parameter (O'Connor & Ott 2011), which attempts to peg the structure outside of the iron core into a single parameter, $\xi_{2.5}$, the inverse of the radius enclosing innermost 2.5 $M_\odot$. A more careful approach to determine the final fates was suggested by Ertl et al. (2016), using both M_4, the mass encompassed at the location where the entropy per baryon equals four, and μ_4, the radial gradient of mass at that location. There is also a more detailed semi-analytical method by Müller et al. (2016) that attempts to capture some of the key ingredients of the core-collapse supernova problem, including the heating, core accretion, shock revival, and neutrino flux, in order to predict the final fates

and masses of the compact remnants. These, and other approaches, have been extensively studied in the context of neutrino-driven explosion scenario (e.g. Ugliano et al. 2012; Pejcha & Thompson 2015; Sukhbold et al. 2016; Ebinger et al. 2019; Mabanta, Murphy & Dolence 2019; Ertl et al. 2020), and our models allow these recent insights to be reflected in BPS calculations.

In this paper, we fill in the evolutionary gap in BPS simulations between carbon ignition and core collapse, in order to explore a more accurate and comprehensive landscape of final fates based on the actual pre-supernova core structure. We evolve the CO cores of massive stars at the time of carbon ignition from a dense grid of initial masses and compositions through core collapse using KEPLER, an implicit hydrodynamics code. Using the structure of the core immediately preceding collapse, we calculate the properties of each model, including the subset of the parameters described above. We discuss these models in detail in Section 2. We present a table of 'explodability' as a function of core mass and starting composition in Section 3. To verify these results, we run a subset of the core models using the open source stellar evolution code MESA (Modules for Experiments in Stellar Astrophysics) and, in Section 4.1, provide comparison with the KEPLER results. As an additional test, in Section 4.2, we compare the pre-supernova properties from the bare CO cores to those from sets of full hydrogenic stars and helium star models depicting stripped cores in close binary systems. We describe the implementation and application of these results in Section 5 and the limitations of our approach in Section 6. Finally, in Section 7, we summarize our results and briefly outline future plans. All of our models are publicly available, and details on how to access them can be found in the Data Availability Statement at the end of this paper.

2 CO-CORE EVOLUTION WITH KEPLER

2.1 Motivations for using CO cores

Simulating cores independently from the rest of the stars for computational studies is not new. Half a century ago He and O cores were being used to investigate the late-stage evolution of massive stars (e.g. Arnett 1972a, b). Initially, cores offered a less computationally expensive means to approximate and probe the intricate physics leading up to core collapse (Nomoto & Hashimoto 1988; Barkat & Marom 1990). While the computational expense is no longer as much of an issue as before (see e.g. Yoon, Woosley & Langer 2010; Sukhbold & Woosley 2014; Woosley 2019, and references therein), the separate treatment of cores remain useful approach because the evolution of the core is not subject to the complete range of uncertainties affecting full stars (see below).

Treating the stellar core in isolation from the rest of the star relies on the 'frozen-envelope' approximation, that the cores are effectively decoupled from their envelopes in the late stages of evolution. With the ignition of carbon, when the central temperature exceeds roughly 5×10^8 K, the stellar core begins to rapidly cool by strong neutrino emission. As a consequence of the temperature sensitivity of neutrino losses, and the need to reach higher temperatures to burn heavier fuels, the evolution of the CO core is drastically accelerated (Woosley et al. 2002). From the ignition of carbon, it takes less than a few thousand years to reach iron-core collapse. The lifetime of the CO core, essentially defined by the carbon-burning timescale, is much shorter than the Kelvin–Helmholtz timescale of the envelope, especially if it is puffy and extended. The stellar envelope hardly has time to respond to the rapid changes in the core, and therefore, the evolution of the envelope is largely disconnected from that of the embedded CO core.

One would expect core-envelope decoupled stars to evolve quiescently from the formation of the core until collapse. Observations of red supergiant supernova progenitors do show that this is the case (e.g. Johnson, Kochanek & Adams 2018), however, not all massive stars go out so quietly. There is clear evidence to suggest that some uncertain fraction of supernova progenitors experience outbursts, some violent, in the millennium preceding core collapse (e.g. Pastorello et al. 2007; Fraser et al. 2013; Mauerhan et al. 2013; Kochanek et al. 2017). Theoretically, it is well established that very massive stars experience late stage instability due to pair production (e.g. Barkat, Rakavy & Sack 1967; Fraley 1968; Woosley 2017, 2019; Marchant et al. 2019). At the lowest masses, the stars may experience instabilities due to silicon flashes (Woosley & Heger 2015), and at intermediate masses, the convective burning episodes in the core during the late stages of evolution may be able to transport significant amounts of energy to the surface by exciting gravity waves (Shiode & Quataert 2014; Fuller 2017; Fuller & Ro 2018). In the absence of such instabilities, however, the CO cores are effectively decoupled from their envelopes.

There are several caveats to our approach. First and foremost, a bare CO core is not a perfect substitute for a core embedded in a full star. Unlike embedded helium cores, there is no steep pressure gradient spanning several orders of magnitude at the boundary of the CO core. The mass of the CO core is not exactly constant (growing due to helium shell burning), and more importantly, the outer parts of real CO cores enclose the deepest parts of the overlaying helium-burning shell. We discuss these issues in further detail in Section 4.2. Secondly, regardless of whether or not the core is embedded in an envelope, its evolution is still sensitive to uncertainties in the input physics, albeit a limited set. For instance, changes in certain nuclear reaction rates (e.g. $^{12}C + ^{12}C$, Bennett et al. 2012) and in the treatment of mixing at the convective boundaries (Meakin & Arnett 2006, 2007; Sukhbold & Woosley 2014) can alter the late stages of evolution by changing the extent, timing, and composition of convective cores and shells. Thirdly, we are not sensitive to any binary interaction that occurs after carbon ignition. While the lifetime of a star is dominated by hydrogen and helium burning, certain rare types of Case C mass transfers could lead to very late mergers, a scenario somewhat similar to the one proposed for the progenitor of SN 1987A (Podsiadlowski, Morris & Ivanova 2007; Menon & Heger 2017). Finally, we do not consider the effects of rotation. We expect rotation to affect the advanced stages of evolution in so far as it changes the CO-core mass and composition prior to carbon ignition. Once carbon ignites, the core evolves too quickly to experience significant structural changes (see fig. 21 of Limongi & Chieffi 2018). Furthermore, models of angular momentum (AM) transport in massive single and interacting binary stars show dramatic AM losses as the stars evolve off the main sequence (Fuller & Ma 2019), further lessening the impact of rotation on late-stage evolution.

Nevertheless, it is the CO core that is at the heart of late-stage evolution. Most physical processes (binary interaction, rotation, mass loss, nuclear reaction rates, etc.), however uncertain, are largely manifested in changing the starting mass and composition of the CO core, which in turn sets its unique evolutionary path until core collapse. Therefore, by evolving a large grid of CO cores until core collapse from varying starting points, we can attempt to effectively link the final pre-supernova structure surrounding the iron core back to the mass and composition of the core at carbon ignition. In conjunction with modern BPS calculations, these results can be used to link the pre-supernova structures to whichever complicated evolutionary pathways produced these CO-core initial conditions.

2.2 KEPLER models

Using the implicit hydrodynamics code KEPLER (Weaver, Zimmerman & Woosley 1978), we run a comprehensive suite of 3496 non-rotating CO cores, each evolved from the ignition of carbon until iron-core collapse. Carbon is ignited roughly when the central temperature exceeds $\sim 5 \times 10^8$ K, and the onset of core collapse is defined as the point in evolution where the infall velocity exceeds 1000 km s^{-1} anywhere in the core. The input physics configurations are largely the same as in Sukhbold et al. (2018). A small 19-isotope network is employed until oxygen depletion in the centre, and a 121-isotope quasi-equilibrium network is used afterwards. We impute a constant boundary pressure of 10^{12} dyne cm^{-2} applied throughout the evolution to simulate the pressure from the overlaying matter. Overshoot mixing is accounted as a slow mixing of zones immediately surrounding regions unstable to Ledoux convection (see section 4.1 of Sukhbold & Woosley 2014). The advanced stage evolution is not expected to be vitally sensitive to rotation (e.g. Heger, Woosley & Spruit 2005; Limongi & Chieffi 2018), and is not considered here. The resolution was mass dependent, and adaptively adjusted during the evolution, but our typical model had about 1200 zones and reached iron core collapse in about 8000 time-steps. We assume that the CO-core mass remains constant and its initial composition is a pure, uniform mixture of carbon and oxygen only. These are reasonable simplifications, since the ultimate goal is to use these results in order to reveal underlying trends in populations of stars, rather than trying to accurately capture the evolution of each individual model.

The CO-core mass, M_{CO}, is varied between 2.5 and 10 M$_\odot$ in increments of 0.1 M$_\odot$. The lower bound is larger than the minimum CO-core mass that can evolve until iron-core formation, estimated to be around ~ 1.4 M$_\odot$, corresponding to ZAMS mass of approximately ~ 9 M$_\odot$ (e.g. Woosley & Heger 2015). We avoid the lightest iron core producing CO cores (< 2.5 M$_\odot$) since they are more degenerate and can be computationally challenging. However most or all of them likely will result in successful supernova explosions, based on simulations of the neutrino driven explosions of light massive stars (e.g. Melson, Janka & Marek 2015; Sukhbold et al. 2016; Burrows et al. 2020; Ertl et al. 2020). The upper limit of our survey, set to 10 M$_\odot$, is well below the limit where the pulsational pair-instability effects become relevant, which is estimated to be around 30 M$_\odot$ by Woosley (2019). In between 10 and 30 M$_\odot$, the CO cores will be very difficult to explode, and they will all likely collapse into black holes, in the neutrino-driven scenario (e.g. Sukhbold et al. 2016; Ertl et al. 2020). As we will show in Section 3, the range between 2.5 and 10 M$_\odot$ captures the region of parameter space where the final outcomes are most likely to vary due to the non-monotonically varying final core structures.

The initial uniform composition is defined by a carbon mass fraction, X_C, which varies from 0.05 to 0.5 in increments of 0.01. As we assume a pure mixture of only carbon and oxygen, the mass fraction of oxygen is $1 - X_C$. In stars, the initial composition of the CO core is almost always oxygen-rich, with $X_C < 0.5$, and the mass fractions are strongly influenced by the competition between 3α and $^{12}C(\alpha, \gamma)^{16}O$ during the preceding core helium-burning phase. The rate of the three-body reaction 3α drops due to the higher entropy in more massive cores, causing the remaining helium to burn via $^{12}C(\alpha, \gamma)^{16}O$ and thus typically, X_C is highest in smaller mass cores and decreases with increasing M_{CO}.

Populations of single stars for a given set of input physics occupy well defined, narrow bands in the X_C–M_{CO} plane (illustrated and discussed further in Section 4.2). For instance, the red supergiant models of Sukhbold et al. (2018) smoothly vary from $M_{CO} = 2.1$ M$_\odot$

and $X_C = 0.25$ to $M_{CO} = 8.2$ M$_\odot$ and $X_C = 0.18$ (their fig. 7). Helium stars evolved with mass loss from Woosley (2019) range from $M_{CO} = 2.3$ M$_\odot$ and $X_C = 0.34$ to $M_{CO} = 12.2$ M$_\odot$ and $X_C = 0.22$ (their figs 7 and 14). The same parameters range from $M_{CO} = 2.0$ M$_\odot$ and $X_C = 0.37$ to $M_{CO} = 33$ M$_\odot$ and $X_C = 0.09$ in the survey on rotating massive star models with enhanced mass loss by Limongi & Chieffi (2018, their fig. 19). These variations are all covered by our grid. Although the extreme cases of high mass and high X_C and low mass and low X_C may not exist in nature, we have attempted to cover a wide parameter space because the outcomes from BPS calculations may occupy a much more diverse region of parameter space than any population of single stars.

3 EXPLODABILITY OF CO-CORES

Two final outcomes dominate the fates of massive stars that experience iron-core collapse: (1) a successful supernova leaving behind a neutron star, and (2) an implosion event without a bright transient that promptly forms a stellar mass black hole. Though there are number of other possibilities, with or without iron-core collapse, they are rare and not expected to significantly influence the overall trends in populations of massive stars. Pair-instability supernovae, which leave behind no remnant, happen only at very high mass, and thus are intrinsically rare. Electron-capture supernovae, which may leave behind a neutron star (or sometimes a white dwarf, e.g. Jones et al. 2016), may happen at lower mass, but the relevant mass range is highly uncertain and could be too narrow to be significant (Jones et al. 2013; Woosley & Heger 2015; Poelarends et al. 2017). Though binary interactions can widen its effective initial mass range, the overall properties of these explosions are not too different from lower energy iron-core collapse supernovae. Additionally, light black holes could be formed through delayed massive fallback in iron-core collapse supernovae, however, recent neutrino-driven explosion surveys indicate that they are infrequent (Ertl et al. 2016, 2020; Sukhbold et al. 2016). Therefore, we only consider the two outcomes that are expected to be the most common: explosions that make neutron stars and prompt implosions that make black holes.

In the most general sense, the existing neutrino-driven explosion surveys indicate that lighter massive stars (corresponding to about 1.4 M$_\odot \lesssim M_{CO} \lesssim 6$ M$_\odot$) tend to explode, while higher mass stars tend to form black holes. The overall fraction of implosions is about ~ 30 per cent in a sample population of single full stars (Sukhbold et al. 2016, 2018), and of mass-losing helium stars that depict stripped cores in close binary systems (Woosley 2019; Woosley, Sukhbold & Janka 2020). The two main outcomes are not cleanly separated in mass space, however. Instead, the results exhibit a complicated explosion landscape (e.g. see fig. 13 of Sukhbold et al. 2016), with 'islands' (in mass-space) of implosions at lower mass, and 'islands' of explosions at higher mass (O'Connor & Ott 2011; Sukhbold et al. 2016). These outcomes are closely correlated with the final core structure, which dictates the dynamics of the ensuing collapse and can directly facilitate or impede the launch of an outgoing shock.

The origin of this complexity is that the characteristics of central carbon burning depend sensitively on the initial conditions of the CO core, and these changes propagate throughout the evolution until collapse to produce drastically different final structures, sometimes even for CO cores that evolved from similar starting points. For a general background on the advanced stage evolution we refer readers to many existing studies (e.g. Woosley et al. 2002; Sukhbold & Woosley 2014; Farmer et al. 2016; Renzo et al. 2017; Sukhbold et al. 2018; Woosley 2019; Sukhbold & Adams 2020). Here, we only

highlight some of the key aspects, and concentrate the discussion on the explodability of CO cores based on their final structures before the collapse. A detailed analysis on the advanced stage evolution will be presented in a separate study.

3.1 Core structure at the onset of collapse

We focus on three, closely related, simple parameters that probe the final core structure: the iron-core mass (M_{Fe}), the mass point where the entropy per baryon (in units of the Boltzmann constant) exceeds four going outward (M_4), and the compactness parameter evaluated at the location enclosing the innermost 2.5 M$_\odot$ ($\xi_{2.5}$, O'Connor & Ott [2011]). For simplicity, we define M_{Fe} to be the enclosed mass where the fraction of silicon drops below 1 per cent, going inward.[1] Generally, stars that form lighter iron cores with a sharply declining external density profile explode more easily. The entropy jump sampled by the M_4 point is almost always carved out by the last oxygen-burning shell, which marks a rapid change in the density profile outside the iron core, and in successful explosion simulations this point strongly correlates with the baryonic mass of the neutron star. Usually stars are easier to explode when the entropy jump is large and is located deep (smaller M_4) in the core. The compactness parameter directly samples the density profile outside the iron core by simply measuring the inverse of the radius enclosing the innermost few solar masses. The value of this parameter is sensitive to the arbitrarily chosen time and mass points of evaluation, 2.5 M$_\odot$ and pre-supernova stage respectively for this study, but the results do not qualitatively change with other choices, that is, higher values correspond to stars more difficult to blow up and vice versa (Ugliano et al. [2012]). All parameters are evaluated at the onset of collapse, when the infall velocity exceeds 1000 km s^{-1} anywhere in the core.

The distributions of these three parameters are illustrated in Fig. 2, all plotted with the same colour contour. A subset of the corresponding numerical values is listed in Table 1. Over the entire range of models, the iron-core masses range from 1.1 to 2.1 M$_\odot$, M_4 ranges from 1.3 to 2.5 M$_\odot$, and $\xi_{2.5}$ is bounded between 0.02 and 0.64. Higher values of all three parameters (darker colours) correspond to CO cores that are more difficult to blow up, and vice versa. The striking similarity of these panels reflect the close correlation between these parameters. With smaller mass iron cores, the external density profile falls off steeply, and the overlaying oxygen-burning shell is located deep in the core. The CO cores that collapse with more massive iron cores have oxygen-burning shells located farther out, and the density outside the iron core remains high. As has been pointed out in prior studies (Sukhbold & Adams [2020], and references therein), higher values of $\xi_{2.5}$ typically correspond to higher M_4, M_{Fe}, and lower $\xi_{2.5}$ corresponds to lower M_4 and M_{Fe}.

These distributions in the X_C–M_{CO} plane are broadly divided into two major regions. At lower initial masses and higher X_C, stars are easier to explode (lower $\xi_{2.5}$, M_4, M_{Fe}) while at higher initial mass and lower X_C (higher $\xi_{2.5}$, M_4, M_{Fe}), stars are harder to explode. These broad regions are separated by a narrow diagonal line stretching from $M_{CO} \approx 2.5$ M$_\odot$ and $X_C \approx 0.10$ to about $M_{CO} = 10.0$ M$_\odot$ and $X_C \approx 0.40$. This diagonal line roughly tracks the starting mass and composition of the CO core where the central carbon-burning transitions from the convective to the radiative regime.

---

[1]The results are nearly identical to the values obtained from alternative definitions, such as those based on infall velocity or the electron mole number profile (e.g. Heger et al. [2001]; Farmer et al. [2016]).
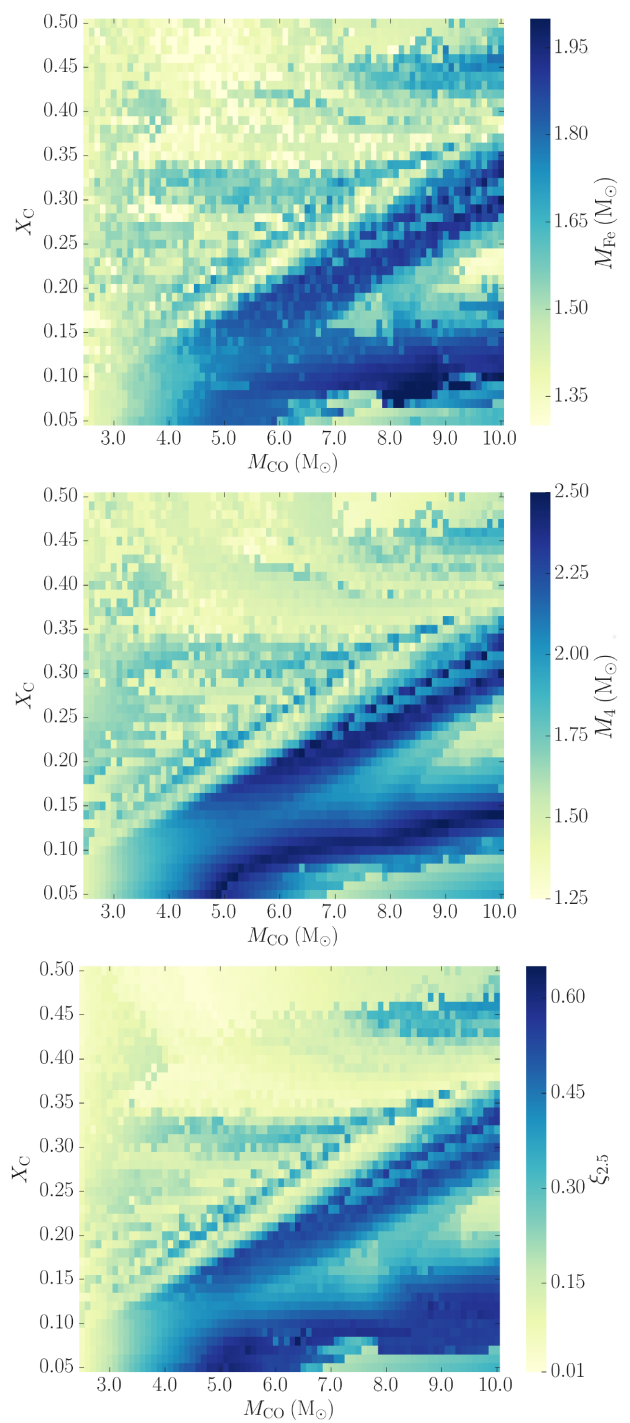

Figure 2. Final core structures from 3496 KEPLER CO-core models with varying mass and initial composition illustrated by their iron-core masses (top), M_4 (middle), and compactness parameter (bottom). The same generic trends in all panels reflect the close correlation between the three parameters; higher values (darker) correspond to cores that are more likely to implode, and lower values (lighter) correspond to cores that are likely to explode. Carbon burns convectively in the centre for models above the diagonal line stretching from $M_{CO} \approx 2.5$ M$_\odot$ and $X_C \approx 0.10$ to about $M_{CO} = 10.0$ M$_\odot$ and $X_C \approx 0.40$.

Table 1. Sample entries from the table of M_{Fe}, M_4, and $\xi_{2.5}$ all evaluated at the onset of collapse, as a function of CO-core mass (columns) and carbon mass fraction (rows) at the time of carbon ignition. The full tables and the final structure and composition for each of the 3496 CO-core models are available online.

$x_C \backslash {}^{M_{CO}}$	$2.5\,M_\odot$	$3.5\,M_\odot$	$4.5\,M_\odot$	$5.5\,M_\odot$	$6.5\,M_\odot$	$7.5\,M_\odot$	$8.5\,M_\odot$	$9.5\,M_\odot$
				$M_{Fe}\,(M_\odot)$				
0.05	1.38	1.58	1.78	1.82	1.50	1.48	1.65	1.62
0.15	1.41	1.52	1.72	1.83	1.78	1.57	1.80	1.77
0.25	1.47	1.56	1.44	1.55	1.39	1.67	1.85	1.54
0.35	1.36	1.33	1.37	1.43	1.43	1.44	1.61	1.66
0.45	1.41	1.35	1.36	1.32	1.45	1.64	1.65	1.76
				$M_4\,(M_\odot)$				
0.05	1.47	1.85	2.28	2.24	1.85	1.63	1.77	1.90
0.15	1.62	1.74	2.16	2.21	2.08	2.06	2.21	2.23
0.25	1.61	1.68	1.71	1.63	1.57	2.00	2.38	1.66
0.35	1.40	1.47	1.40	1.55	1.43	1.44	1.94	1.76
0.45	1.46	1.44	1.50	1.29	1.46	1.73	1.77	1.84
				$\xi_{2.5}$				
0.05	0.06	0.30	0.51	0.59	0.38	0.22	0.26	0.31
0.15	0.08	0.20	0.48	0.47	0.35	0.30	0.45	0.50
0.25	0.08	0.20	0.19	0.21	0.13	0.38	0.53	0.27
0.35	0.05	0.07	0.06	0.09	0.06	0.06	0.35	0.26
0.45	0.04	0.06	0.04	0.04	0.14	0.25	0.33	0.37

Carbon burns convectively in the centre in the models above this line, and it burns as a radiative flame below. To drive a convective episode, the energy losses due to neutrinos needs to be exceeded by the local energy generation rate from carbon burning, which depends on both the initial mass and composition of the CO core. At low X_C, the CO core is essentially an oxygen core. There is little carbon to burn, let alone to drive a convective episode. At higher CO-core masses, higher carbon mass fractions are required to sustain convection during central carbon burning, causing the upward diagonal trend. When carbon burns radiatively in the centre, its entropy is higher because it effectively skips the long lasting neutrino-cooling phase. In higher entropy cores, oxygen generally burns in a very massive convective episode, which ultimately forms a massive iron core with a shallow external density profile (for a detailed discussion see Sukhbold & Woosley 2014; Sukhbold & Adams 2020).

Although this transition is a major inflection point, it is not the only property of central carbon burning that controls the final core structures. The timing and the mass extent of the convective burning episode or the radiative flame also depends on the starting mass and composition of the CO core. These changes then affect the timing and extent the next shell and core-burning episodes and can propagate throughout the evolution to drastically change the final structure at the onset of core collapse, even in cores that started from nearly identical initial conditions. These effects are illustrated through the models located below the diagonal line that are easier to explode (lower $\xi_{2.5}$, M_4, M_{Fe}), and models above the line which have higher $\xi_{2.5}$, M_4, M_{Fe}. Notice those dark 'streaks' in models with convective central carbon burning, and prominent bright 'valleys' of low values that cut through the dark, high-valued models with radiative carbon burning. The main 'valley' which roughly lies along the line running from $M_{CO} = 3$, $X_C = 0.05$ to $M_{CO} = 10$, $X_C = 0.25$ is caused by a modulation between the carbon-burning shell and the oxygen-burning core. For these conditions, the carbon burns in a shell located just outside the effective Chandrasekhar mass and prevents the development of a massive oxygen-burning core. A lighter oxygen-burning core then results in a lighter iron core. The smaller 'valley,' represented by the most massive ($M_{CO} > 7\,M_\odot$) oxygen-rich CO cores ($X_C < 0.1$), is caused by the same effect,

but, in this case, the oxygen-burning shell impedes the development of massive silicon-burning core, which again results in a lighter iron core. The existence and scope of some of these details are sensitive to the adopted convective mixing physics (Sukhbold & Woosley 2014; Sukhbold et al. 2018).

3.2 Assessing the final fates: explosion versus implosion

As our understanding of the neutrino-driven explosion mechanism has not fully converged (see review by Janka, Melson & Summa 2016), and given the uncertainties of stellar evolution (Section 2.1), currently there is no simple parameter that definitively predicts the final fate of a massive star based on its final core structure. However, we can employ some of the existing neutrino-driven explosion surveys to infer the general trends for populations of massive stars.

As a sample case, here we use the 'Ertl criterion', developed to reproduce results based on a large number of calibrated 1D explosion simulations of massive stars (Ertl et al. 2016, 2020). This method employs a combination of two parameters to probe the final core structure, M_4, and the radial gradient of mass at that location, μ_4. The μ_4 parameter correlates with the mass accretion rate on to the shock and depends on the steepness of the entropy jump at the location of M_4. The explosion criterion is defined as the line $\mu_4 = k_1 M_4 \mu_4 + k_2$, where k_1 and k_2 are constants. We use the updated calibration for the N20 engine with $k_1 = 0.182$ and $k_2 = 0.0608$ (Ertl et al. 2020). The radial gradient is evaluated within $0.3\,M_\odot$ of M_4 (equation 6 in Ertl et al. 2016). All cores with μ_4 values above the line form black holes and cores with μ_4 below the line die in a supernova explosion.

The final fates of our models based on the Ertl criterion are shown in Fig. 3, with light boxes representing explosions and dark boxes representing implosions. The models which implode largely trace those with high values of $\xi_{2.5}$, M_4, M_{Fe}, and vice versa, roughly following the generic trends seen in Fig. 2. The diagonal line tracing the transition of the central carbon burning stands out, and we find three distinct 'islands' of explodability that roughly correspond to the 'valleys' of Fig. 2. Many of these detailed features above and below the carbon-burning transition line are not absolutes, and their properties can change depending on the criterion used to determine
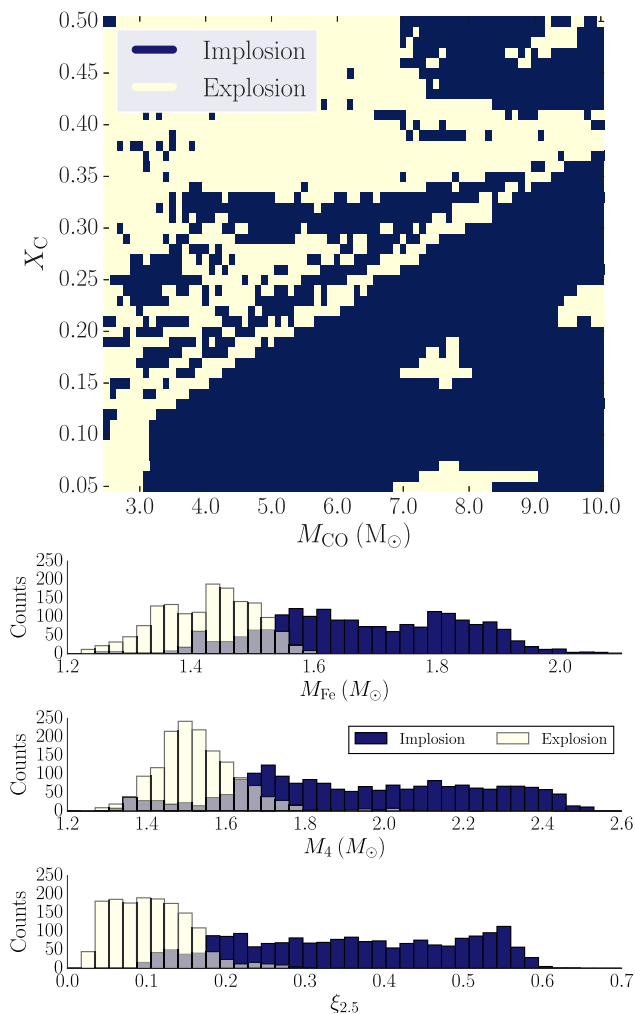
Table 2. Critical values based on sample explosion criterion.

	M_{Fe} (M$_\odot$)	M_4 (M$_\odot$)	$\xi_{2.5}$
		Explosion	
Min	1.10	1.25	0.02
Max	1.74	2.10	0.30
		Implosion	
Min	1.24	1.33	0.04
Max	2.10	2.52	0.64
		Cross points	
	1.54	1.66	0.18

Note: 'Cross points' refers to value at which the two distributions cross (see Fig. 3).

Figure 3. Top: a distribution of the models in the X_C–M_{CO} plane which explode (pale yellow) and implode (dark blue) given a sample explosion criterion from Ertl et al. (2016, 2020). The results closely follow the trends seen in Fig. 2, with imploding models tracking higher values of $\xi_{2.5}$, M_4, M_{Fe}, and vice versa. The final outcomes are closely correlated with final core structure and sensitively depend on both the mass and initial composition of the CO core. Bottom: histograms for each parameter evaluated at collapse showing the distribution of values for the models which explode (pale yellow) and implode (dark blue). The crossing points (Table 2) of these distributions roughly represent the final structure of models near the central carbon-burning transition, and near the critical line of the adopted Ertl criterion.

separate *most* of the explosions from *most* of the implosions. They roughly track the final core structures near the central carbon-burning transition line and also the critical line separating the two outcomes in the Ertl criterion (Sukhbold & Adams 2020). Although these values are not too different from the limits and cutoffs discussed in earlier studies (e.g. Mazurek 1982; Woosley & Weaver 1995; O'Connor & Ott 2011; Horiuchi et al. 2014), we again stress that these should not be taken as absolutes.

Here, we demonstrate the evaluation of final fates using a sample criterion for explosion. The full tables containing our numerical results, including μ_4, though it is not listed in Table 1, as well as the structure and composition of each pre-supernova core are available for download (see Section 8 for details). Readers can take these models and apply their preferred calibrations and criteria for determining a star's final fate. Though the results may change from what is presented here, the bulk trends should stay the same.

4 VALIDATION OF RESULTS

In order to confirm our approach, we recreate the KEPLER calculations presented in (Section 3) with an independent open source stellar evolution code, and also compare our results with full star and helium star models that embed equivalent CO cores. A good overall qualitative agreement is found in both comparisons. There are differences, however, that point to the limitations of our approach, and highlight that these results should only be used to infer the overarching trends in populations of stars rather than individual models.

4.1 Comparison with MESA

We employ version 7624 of MESA (Paxton et al. 2010, 2011, 2013, 2019) to create an equivalent suite of CO-core models. As with the KEPLER grid, the constant CO-core mass ranges between 2.5 and 10 M$_\odot$, and the initial uniform composition ranges between 0.05 and 0.5 in X_C. Although we maintained the same mass increments (0.1 M$_\odot$), a larger compositional increment was used (0.05 instead of 0.01) for quicker computation. This leads to 760 non-rotating CO-core models all evolved from carbon ignition until core collapse, which is defined the same way as in KEPLER models. We also employed a small 22-isotope nuclear reaction network. We emphasize that no attempts were made to mimic the results from KEPLER, though it is possible (e.g. section 4 of Sukhbold & Woosley 2014). The input configurations, including the convective overshoot mixing setup, are fairly similar to those in recent studies of massive stars (e.g. Farmer et al. 2016), although the tolerances for changes
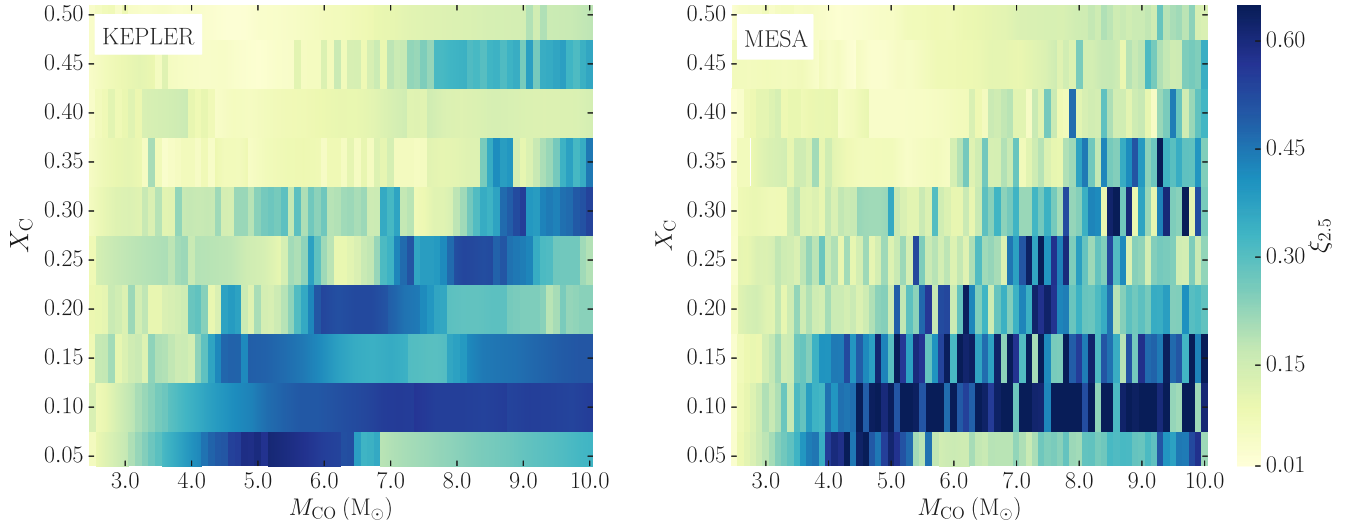
final fate as well as the input physics of the models. With a weaker engine the 'islands' may almost disappear, while with a stronger engine they will broaden and merge into valleys of lower values, and the dark patches above the diagonal line will diminish. However, nowhere in this distribution can a line be drawn that cleanly separates the two outcomes, which clearly demonstrates that final fates depend on both M_{CO} and X_C.

The bottom panel of Fig. 3 shows the distributions of the two outcomes for each parameter, with their respective numerical values listed in Table 2. With the adopted prescription, no explosions occur for $\xi_{2.5} > 0.3$, $M_{Fe} > 1.6$ M$_\odot$, and no implosions for $\xi_{2.5} < 0.1$, $M_{Fe} < 1.35$ M$_\odot$. The M_4 values are appreciably more spread out, but generally, there are hardly any explosions above $M_4 > 1.8$ nor implosions below $M_4 < 1.3$ M$_\odot$. The crossing points of these distributions, $\xi_{2.5} \sim 0.18$, $M_4 \sim 1.66$M$_\odot$, $M_{Fe} \sim 1.54$ M$_\odot$,

Figure 4. The compactness parameter ($\xi_{2.5}$) evaluated at core collapse for our KEPLER models (left) and 760 MESA models (right). The KEPLER models are the same as those in the bottom panel of Fig. 2, but we only display those with equivalent X_C to the MESA models for the sake of comparison. Similar general trends are evident in both suites, including the upward diagonal line marking the transition of central carbon burning, and 'valleys' of lower $\xi_{2.5}$ beneath this line. A comparison of M_4 and M_{Fe} show similar behaviour and agreement between two codes.
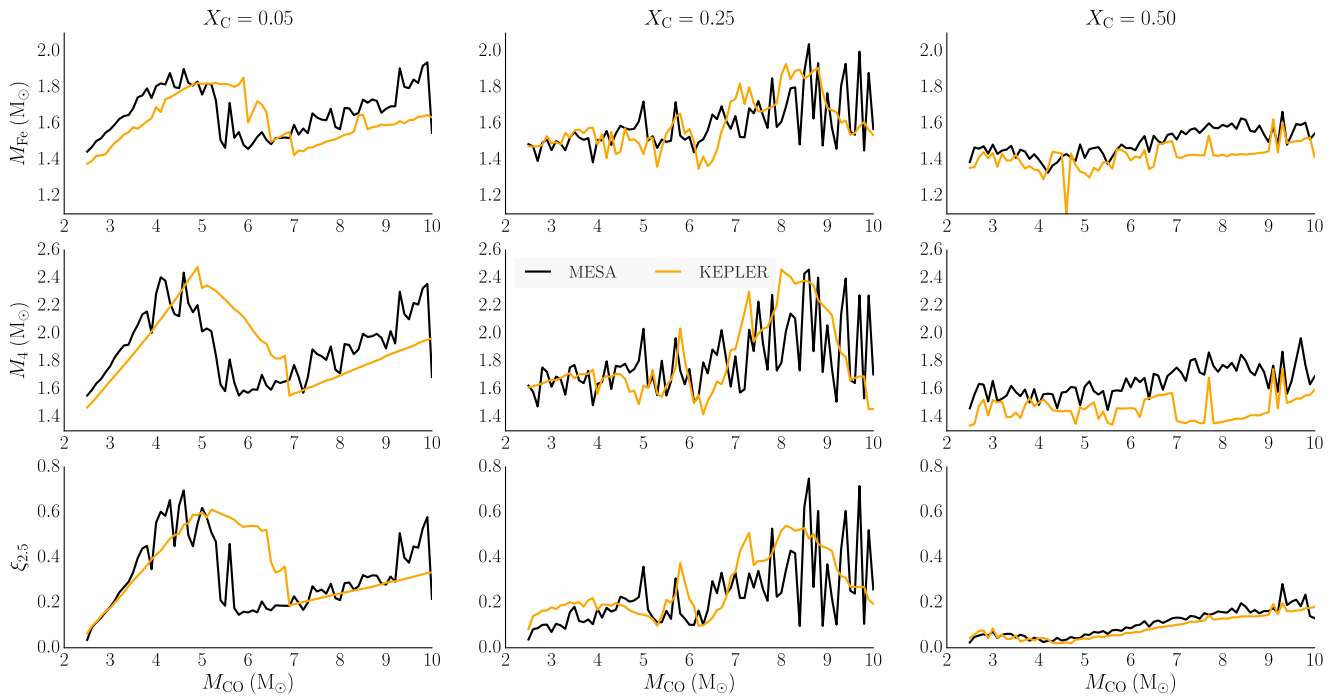
Figure 5. Comparison between KEPLER (orange) and MESA (black) results for all three parameters evaluated at core collapse (rows) for fixed initial carbon fractions (columns, $X_C = 0.05, 0.25, 0.50$). Since the CO-core mass increments were identical, there are 76 models per code in each panel. Despite the slight shifts in the structures due to different treatments of convective mixing, and higher oscillations in MESA models due to the use of higher tolerances in the calculations, the general trends are in good overall agreement.

in stellar properties between time-steps have been generally relaxed in order to smoothly achieve iron-core formation in large number of many models. The input file (inlist) is included in the online data release (see Section 8 for details).

Fig. 4 compares the compactness parameter ($\xi_{2.5}$) evaluated for the KEPLER (same as in Fig. 2) and MESA models. The overall good agreement between the two is evident. The MESA models show the same regional trends in this parameter space: a darker region

and a lighter region separated by an upward diagonal line, where carbon burns convectively in the centre above it, and radiatively beneath it. The 'valleys' beneath the central carbon-burning transition line (Section 3.1) for higher mass cores ($M_{CO} > 5\,M_\odot$) with lower initial carbon mass fraction ($X_C < 0.3$) also fall roughly in the same place. These results indicate that the structure of the pre-supernova cores are similar, despite the different codes and input configurations. Although only the compactness parameter is shown in Fig. 4, the
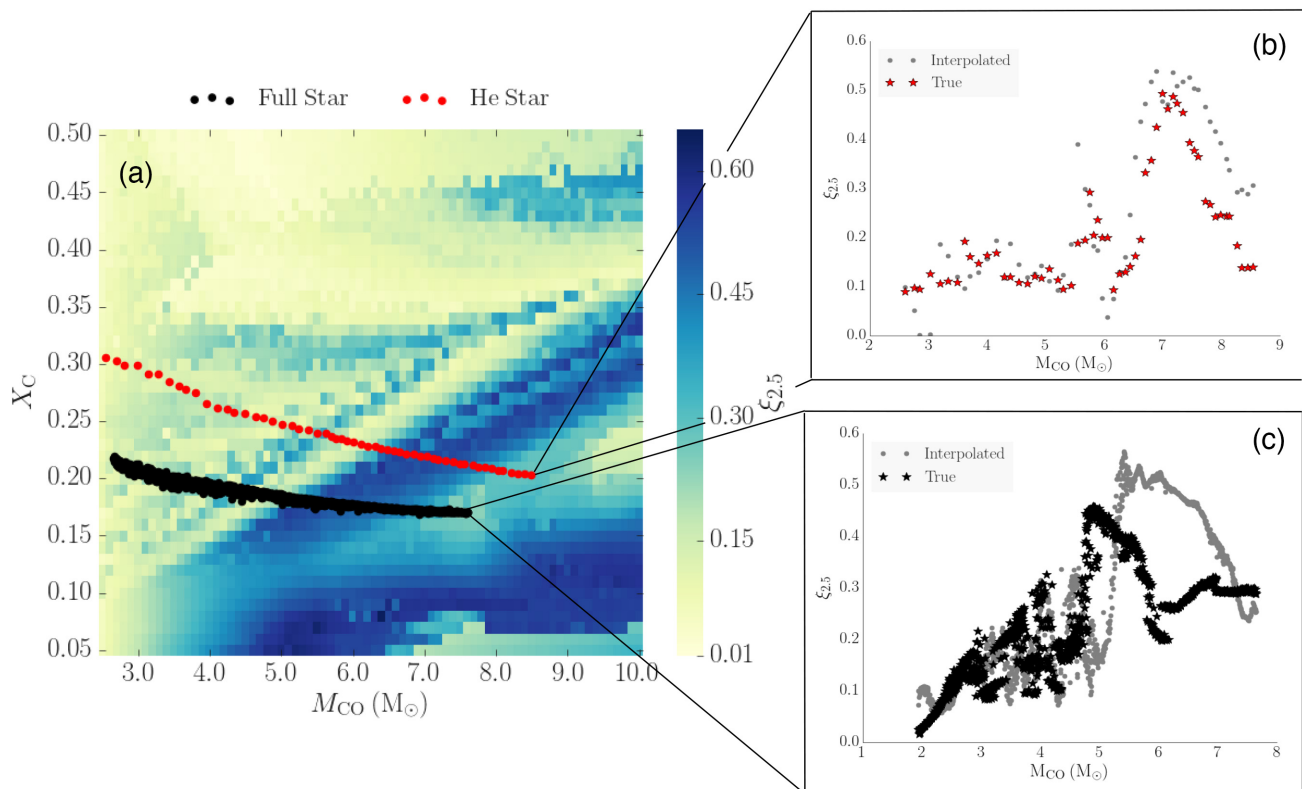
Figure 6. Panel (a) shows the core parameters from full stars (black) and He stars (red) superimposed on the $\xi_{2.5}$ distribution (same as in Fig. 2). For a given set of single star models, the CO cores start out with more oxygen with increasing mass. Panels (b) and (c) compare the values of $\xi_{2.5}$ for the full and He star models calculated directly from the stellar pre-supernova core properties and those interpolated from our tables. While the height and width of the peak in $\xi_{2.5}$ at higher core masses varies between the true and interpolated values, the bulk trends remain the same.

same good qualitative agreement is also found for the iron-core mass and M_4.

A more detailed comparison is presented in Fig. 5, where all three parameters are compared for different compositions of $X_C = 0.05$, 0.25, and 0.50. Since the mass increments were identical, there are 76 models per code in each panel. Though the general trends are in good agreement, the final structures for oxygen-rich CO cores in MESA (low X_C) move to the 'valley' (Section 3.1) at lower core mass than the KEPLER models. At higher X_C, the M_4 values and iron-core masses in the KEPLER models are often lower, indicating a deeper location for the last strong oxygen-burning shell. These systematic differences can be largely attributed to the different treatment of convective mixing, which is set to be more efficient in the MESA models (for the sensitivity, see Sukhbold & Woosley 2014). Also the MESA solutions generally exhibit larger irregularities and oscillations for all masses and compositions. This is due to the much larger tolerances adopted for the calculations.

4.2 Comparison with full stars and He cores

To further gauge the validity of our approach, we compare our results to the CO cores in the suite of single star models from Sukhbold et al. (2018) and He star models evolved with mass loss from Woosley (2019). The single stars consist of 1500 models with initial masses ranging between 12 and 27 $M_\odot$, all of which retained a significant hydrogen envelope (e.g. died as red supergiants). Their embedded CO cores marginally grow in mass due to the overlaying helium-burning

shell. In contrast, the helium stars represent stripped He cores of massive stars in close binary systems, where the entire hydrogen envelope is removed near the time of helium ignition at the centre. The set had 56 models with *initial He-core* masses between 5.00 and 18.75 $M_\odot$. These cores evolve by losing mass in winds, and with their adopted prescription, the embedded CO cores were exposed before the collapse for He cores that had initial masses more than about 17 $M_\odot$ ($M_{CO} \sim 7\,M_\odot$). Both sets of models were computed with KEPLER and had similar input physics to the models presented in this study.

To make the comparison, we first map these models in the X_C–M_{CO} plane by measuring the carbon mass fractions and CO-core masses for each model when the central temperature reaches 5×10^8 K (central carbon ignition). The composition is well mixed by the prior convective helium-burning core and thus there is no ambiguity in measuring X_C. However, the mass of the CO core can be sensitive to how one determines its outer boundary. The boundary of M_{CO} is usually measured at the location where the mass fraction of ^{4}He drops below 1 per cent going inward. This threshold generally works, but it can significantly underestimate the CO-core mass in cases where the ^{4}He profile exhibits an extended tail deep into the core. A higher threshold of 20 per cent or 50 per cent would typically coincide with the outer boundary of the helium-burning shell, but it can also overestimate the M_{CO} in some rare cases. Given these considerations and the simple nature of our models, we chose to measure the CO-core mass as the average of the masses inside the 1 per cent and 25 per cent thresholds.

The results are illustrated in panel (a) of Fig. 6. Both sets of models occupy a well-defined narrow band where the CO cores begin their evolution with more oxygen (lower X_C) with increasing mass, due to the dominance of $^{12}C(\alpha, \gamma)^{16}O$ over 3α during the prior helium-burning phase. The single star models span up to about $M_{CO} \sim 7.5 \, M_\odot$, while the helium stars reach nearly 9 $M_\odot$. The initial compositions are drastically different, however, due to the receding convective helium-burning core in the mass-losing helium star models (Woosley 2019). Unlike embedded helium cores, which grow in mass, the shrinking convective core leaves behind a gradient of carbon, brings no extra helium into the burning shell, and results in less destruction of carbon. Both sets of models used a rate for $^{12}C(\alpha, \gamma)^{16}O$ equivalent to about 1.2 times the rate by Buchmann (1996).

Based on the location of these models in the X_C–M_{CO} plane, we obtain their corresponding final core structure properties by linearly interpolating on our grid of CO-core models. The results comparing the final compactness parameter (outcomes are similar for M_{Fe} and M_4) are shown in panels (b) and (c) of Fig. 6. The agreement with He star set is excellent (panel b), where the integrated values of $\xi_{2.5}$ stay low until about $M_{CO} \sim 6 \, M_\odot$, after which the CO cores burn carbon radiatively in the centre and form the peak of $\xi_{2.5}$. Though it is slightly broader and taller, the interpolated values peak at the same mass $M_{CO} \sim 7 \, M_\odot$ and at similar $\xi_{2.5} \sim 0.5$. The agreement with full stars (panel c) is good until the embedded cores transition to radiative carbon burning at about $M_{CO} \sim 4.5 \, M_\odot$, however, the same transition happens in bare cores at a slightly larger mass. As a result the peak is shifted by about a solar mass, but it is much broader in bare CO cores. For both of these cases, the interpolated values closely track these models especially at lower mass, and over the entire comparison grid it exhibits qualitatively same non-monotonic variation with a distinct peak.

While this result is highly encouraging, there are some discrepancies which directly point to the limitations of our approach. Fig. 6 shows that the values of $\xi_{2.5}$ show the biggest differences at higher CO-core masses. At a given central temperature, our bare cores are denser in the centre and cooler in the outer parts compared to their equivalent embedded cores. In bare cores, the carbon ignites slightly earlier with a higher energy generation and smaller neutrino loss rates. The change in the central carbon burning in turn starts a ripple effect by modifying the timing, location, and the extent of the next shell and core-burning episodes. Higher mass cores are most sensitive to these changes since carbon burns radiatively in the central core with a very short lifetime as compared to lower mass cores with long lasting convective burning. These are not only the consequences of the artificially constant mass and boundary pressure in our models, but are also influenced by the intrinsically different outer structure. There is no helium-burning shell in bare CO cores, and the strength of the outermost carbon-burning shell is often very different than in the embedded counterparts. In a sense, the final core structure in *bare* CO-cores changes more slowly with increasing mass compared to embedded cores, and hence forms a much broader $\xi_{2.5}$ peak. This effect is more pronounced for full stars, and it is only mildly present with He stars.

Though the calculated and interpolated values of $\xi_{2.5}$ are not in full agreement with one another, they do follow the same overall trends. However, these simple, first iteration, CO-core models should not be used to infer the pre-supernova structure of any given stellar model, and instead, should only be applied to populations of massive stars in order to infer the underlying trends in the properties of their final demise.

5 IMPLEMENTATION

The application of our approach requires knowledge of the CO-core mass and its initial carbon mass fraction for each model. BPS calculations that employ stellar evolution codes often reach the central carbon-burning phase, and both CO-core properties can be extracted. In these cases our tables can be used directly to infer the core structure at the onset of collapse, and below we provide a sample application to recent results on Type-IIb supernova progenitors. Our results cannot be directly applied to 'rapid' BPS calculations, in which only the CO-core mass is tracked, but not its starting composition. At the end of this section, we discuss possible ways to approximate X_C in such scenarios.

5.1 Sample application: progenitors of Type-IIb supernovae

Given the simplistic nature of existing prescriptions used to determine the final fates of stars, we expect the outcomes of many BPS studies to be affected by our results. As a test case, we apply our calculations to a recent study on Type-IIb supernova progenitors by Sravan et al. (2019). Using MESA, they have simulated a large population of single and binary models and find, among other things, that the binary channel dominates at low metallicity and may fully account for the observed rate of Type-IIb events. A full description of their parameter space is listed in their table 1, but in summary, binary models were explored within primary ZAMS masses of $1.0 < \log M_1 < 1.4 \, M_\odot$, mass ratios of $0.225 < q < 0.975$, mass transfer efficiencies of $0.01 < \epsilon < 1.0$, initial orbital periods of $1.0 < \log P < 3.8$ d, and metallicities of $Z_\odot$ and $Z_\odot/4$. For solar metallicity models, the span in initial period is reduced to $2.5 < \log P < 3.8$ d. To be considered an interacting binary system in their study, the primary star must lose at least 1 per cent of its initial mass to Roche lobe overflow. All primary stars which reached central carbon depletion while retaining hydrogen envelopes with masses between 0.01 and 1 $M_\odot$ were designated as Type-IIb progenitors.

To produce a Type-IIb supernova, the progenitor star not only needs to reach core collapse with the right envelope properties, but the collapse ultimately needs to produce an explosion. Although the upper bound on M_1 ($\sim$25 $M_\odot$) in their grid excludes most stars that would be difficult to explode with neutrinos, it does include many stars that are likely to implode, and thus, would not produce a Type-IIb despite having the right envelope mass. We test this by recomputing a sample subset of their population at a fixed mass ratio ($q = 0.925$) and mass transfer efficiency ($\epsilon = 0.1$), using the same version of MESA (9575). Since the lightest CO cores produce explosions over a wide range of initial compositions, we only explore primary stars more massive than about 14.5 $M_\odot$ (roughly corresponding to $M_{CO} \sim 3 \, M_\odot$). Otherwise we probe their entire parameter space in mass and orbital period using increments of 0.04 and 0.05 dex, respectively, about double the increments used in their paper, which they note should not affect the results.

All models were terminated at either carbon ignition or when the envelope mass dropped beneath 0.01 $M_\odot$. The former is slightly before the evolutionary cut-off used in Sravan et al. (2019, carbon depletion), but due to the negligible mass lost during carbon burning, our results are nearly identical to theirs. Following the Sravan et al. (2019) criteria, the models which retained a hydrogen envelope of 0.01–1 $M_\odot$ at carbon ignition and lost at least 1 per cent of the primary star's initial mass to Roche lobe overflow were designated as binary Type-IIb progenitors. We then took the core properties, M_{CO} and X_C, at carbon ignition and rounded to the nearest discrete point in our
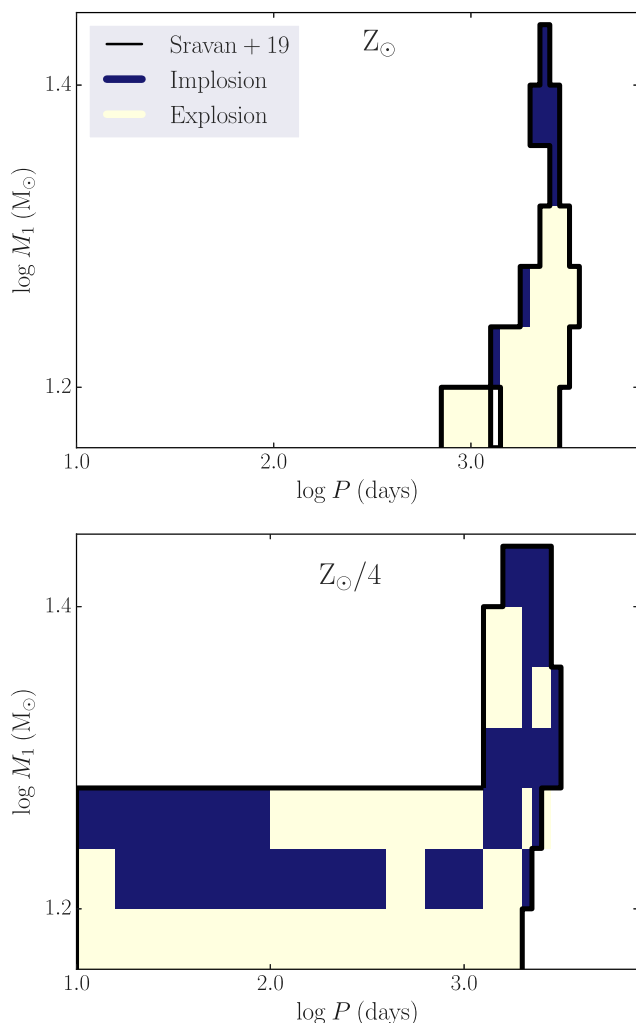
Figure 7. The regions of the primary mass–binary orbital period parameter space which produce Type-IIb supernova progenitors using the criteria in Sravan et al. (2019, outlined in black) and our core models (light bars explode and dark bars implode). The top panel shows the results for solar metallicity models and the bottom shows $Z_\odot/4$ models. Given the pre-supernova structures inferred from our CO-core models, and the application of a sample explosion criterion on them, we find that significant fraction of stars that collapse with the right hydrogen envelope mass may not be likely to produce a Type-IIb supernova explosion.

grid of final fates from Fig. 3, adopting the outcome of that point. As in Section 4.2, we take M_{CO} to be the average of the 1 per cent and 25 per cent threshold masses.

Fig. 7 shows the results from both the Sravan et al. (2019) criteria and our CO-core models. The areas outlined in black highlight the region of the parameter space which produce Type-IIb supernovae according to the Sravan et al. (2019) criteria. At solar metallicity (top panel), progenitors with low-mass envelopes form exclusively in wide systems, while at lower metallicity (bottom panel), they can form in shorter period systems due to weaker envelope expansion and winds. These results fully match their results (see their figs 4 and 5). However, we find that only a subset of these models produce supernova explosions when we consider their presupernova core structures based on our CO-core models and apply the same sample explosion criterion from Section 3.2. All light coloured regions enclosed in the outlined areas explode and all darker regions implode.

The most massive models, at both metallicities, have radiative central carbon burning and result in implosion as they lie beneath the diagonal line in the X_C–M_{CO} plane. Lighter models with convective central carbon burning generally explode, but at low metallicity, many of the shorter period stars do not explode as they cross the region just above the diagonal line where the final outcomes are uncertain (see Section 3). By number, we find roughly a fifth of the models in our small grid implode at $Z_\odot$, and roughly half at $Z_\odot/4$.

Although one needs to examine other combinations of q and ϵ, and apply proper initial mass function weighting, these results already pose potential challenges to some of the findings by Sravan et al. (2019). For instance, the observed rate of Type-IIb events is unlikely to be fully accounted for by low-metallicity systems, even with low mass transfer efficiency because many of these primary stars implode instead of explode. The relative contributions from single and binary channels, and its dependence on metallicity, could be be significantly different as well.

5.2 Only having M_{CO}

The rapid BPS codes (e.g. Giacobbo & Mapelli 2018; Breivik et al. 2019) approximate stellar evolution through the fits by Hurley et al. (2000, 2002), which only compute the CO-core mass instead of both mass and composition. The relation between initial carbon mass fraction and M_{CO} is sensitive to the input physics operating during the prior evolution (e.g. reaction rates, mixing, rotation, and mass loss/transfer), and it cannot be reliably approximated, especially for populations spanning different metallicities. The ideal solutions are to incorporate a dedicated prescription in the BPS code to track X_C or to map it by employing stellar evolution calculations for a subset of the population.

A very basic approximation may be made by utilizing the existing single star models and by assuming that the relation between X_C and M_{CO} changes only depending on whether the He core in each star was embedded or exposed during the evolution. For example, the solar metallicity single star models from Sukhbold et al. (2018) and helium stars evolved with mass loss from Woosley (2019) give (see Fig. 6a)

$$X_C = 0.20/M_{CO} + 0.15 \tag{1}$$

for single stars and

$$X_C = -0.084 \times \ln(M_{CO}) + 0.4 \tag{2}$$

for mass losing, bare, helium stars.

The initial carbon mass fractions for stars that have lost their envelopes through binary interaction could be estimated by using the relation based on mass-losing, helium star models, and the relation based on full star models could be used for all other stars in which the He cores were always embedded. However, such an approximation is highly simplistic, and completely ignores the fact that even for single stars the relation between X_C and M_{CO} can appreciably change due to uncertain input physics and variations in metallicity. The relation is further complicated through certain binary interactions (e.g. post-main-sequence mergers), and ultimately, the ability to track X_C is needed in rapid BPS models for a more accurate description of stellar final fates.

5.3 Beyond final fates

While in this study we focus on the final fates, our results can be utilized to infer other properties. For example, the pre-supernova structures can be used in conjunction with some explosion criterion

to approximate the compact remnant mass. When a star explodes based on its embedded CO core, the baryonic mass of the resulting neutron star could be approximated by M_4. When the embedded CO core is deemed to implode, the resulting black hole mass could be bracketed as the helium core mass at the evolutionary cut-off, as a minimum, plus some uncertain but small fraction of the surviving envelope (if the star retains some envelope) as a maximum. These results also could be used to infer the nucleosynthesis, however, this requires a coupling to an explosion modelling, and will be explored in a forthcoming study.

6 DISCUSSION

The exploration of the CO-core evolution as a bridge between the end of BPS simulations and the end of a star's life is a step forward in improving the outcomes of BPS models. However, this approach is not without its caveats, and below we briefly comment on some of the key concerns.

There is a considerable agreement among the 1D models of advanced stages of evolution from independently developed stellar codes (Sukhbold & Woosley 2014; Chieffi & Limongi 2020; Schneider, Podsiadlowski & Müller 2020), especially concerning the broad variation of the final core structure in mass space. We explicitly demonstrate this feature between the two codes used in this study for CO cores spanning wide range of initial conditions (Section 4.1). Also the advanced stages of evolution are probably not too sensitive to some of the ingredients ignored in this study, like the mass gain/loss and rotation. The evolutionary timescales are just too short for any appreciable change in core mass, or for rotationally induced instabilities to set in (e.g. Heger et al. 2005; Limongi & Chieffi 2018). However, there are important differences in the details. Perhaps the most important uncertainty affecting all of the existing models is the treatment of mixing, especially at the boundaries of convective regions. Small changes in the timing and location of convective shells, say during C burning, can have a drastic effect on the final core structure, and therefore, the final explodability. Although limited in their scope, earlier (e.g. Meakin & Arnett 2007; Viallet et al. 2013) and more recent multidimensional simulations (e.g. Fields & Couch 2020; Yadav et al. 2020) all suggest possible significant departure from the mixing length theory.

Individual models are obviously sensitive to the numerical setup as well. Changes in the size of the nuclear reaction network, the choices on spatial and temporal resolution all affect the final outcome of a given model (for individual variations see Farmer et al. 2016). However, Sukhbold et al. (2018) noted the possible inherent chaos stemming from the advanced stages of evolution itself, and argued that large variations in the core structure are expected in a wide range of masses no matter what resolution or reaction network is employed in the calculation. Therefore it makes sense to study wide ranging models, as we did in this study, to explore the overarching characteristics that are essentially statistical in nature, rather than trying to accurately model each individual core. This sensitivity to the initial conditions is manifested as rapid variations in the final pre-supernova structures across models starting from similar masses and compositions (see discussion in Section 3), and was seen and reported in several prior studies involving KEPLER and MESA models (Woosley et al. 2002; Sukhbold & Woosley 2014; Müller et al. 2016). This apparent 'chaos' is not seen in all codes (e.g. Chieffi & Limongi 2020), and its existence and extent certainly warrants further quantitative work.

Knowing the pre-supernova core structures allows one to utilize modern insights on the mechanism of core-collapse supernova

explosions. While these insights have a higher pedigree than simpler inferences just based on the CO-core mass (e.g. Fryer et al. 2012), they are still simplistic and very much uncertain. The results based on 1D calibrated neutrino-driven explosion simulations by Ertl et al. (2016, 2020, discussed in Section 3.2) are broadly in good agreement with that of Müller et al. (2016) and Pejcha & Thompson (2015), however, there are number of other approaches (e.g. Mabanta et al. 2019; Couch, Warren & O'Connor 2020) that have not been carefully compared. Some of the ab initio multidimensional simulations are starting to produce successful explosions across a wide range of stellar masses (e.g. Burrows et al. 2020), but the outcomes are fairly sensitive to progenitor perturbations and rotation (e.g. Vartanyan et al. 2018), and currently there is only a limited consensus (O'Connor et al. 2018). There is of course the more fundamental question of whether most core-collapse supernovae are powered by neutrinos. Recent studies indicate difficulty in reaching explosion energies well above 2×10^{51} erg (e.g. Ertl et al. 2020), and the neutrino-driven mechanism is likely inadequate to explain rare and energetic events like gamma-ray bursts and superluminous supernovae.

Finally, with regards to implementation of our approach, one might question the efficacy of combining stellar models computed with different codes, each with their own set of assumptions and input physics. While self-consistent population models capturing the evolution from birth to death is ultimately warranted, we do not believe this would be a major issue, especially when it comes to estimating only the bulk trends in core structure and final fates. Having some form of description for the advanced stages of evolution and the corresponding pre-supernova core structure is more useful than completely ignoring these. We also note that one does not have to completely rely on our models; when feasible, one can and should roughly follow our recipe and compute a grid of CO cores with their own code and choices of input physics.

7 CONCLUSIONS

Knowing the final fate of the star is critical in any population study involving massive stars. Only exploding stars produce bright supernovae, substantially contribute to nucleosynthetic yields, and dissolve binary systems. The final fate of the massive star, whether it explodes or implodes, is dependent on its core structure right before the collapse. However, the majority of current population synthesis calculations follow the evolution of stars only until central carbon burning (Fig. 1), and without knowing the final pre-supernova structure, assume final fates from simplified prescriptions.

In this study, we explore one potential solution to this problem by treating the CO cores independently from the rest of the star. Through an extensive suite of bare CO-core models, each evolved from central carbon ignition until the onset of core-collapse, for the first time we map final pre-supernova core structures to a diverse set of CO-core initial conditions. These models reasonably mimic the embedded CO cores of massive stars, and can be utilized in single population synthesis and/or BPS calculations to infer the final fates and the remnant properties based on the pre-supernova core structure. We summarize the main results as follows:

(i) Our main grid consists of 3496 models computed with the implicit hydrodynamics code KEPLER. For simplicity, the mass of the CO core was assumed to be constant and all models start from a uniform mixture of carbon and oxygen only. The range of initial compositions ($0.5 > X_C > 0$) encompasses nearly all combinations possible in nature, while the mass was confined between 2.5 and $10\,M_\odot$. All lighter CO cores that reach iron-core collapse will likely

produce a supernova explosion no matter the starting composition, while all heavier cores will implode until the onset of pair-instability effects. Our grid captures the mass range where the final core structure, and therefore the final fate of the core, varies the most depending on its initial composition.

(ii) We have explored the pre-supernova core structures by focusing on three simple parameters – M_{Fe}, M_4, and $\xi_{2.5}$. In the X_C–M_{CO} plane, all three parameters exhibit similar trends reflecting their close correlation (Fig. 2). They show that the final core structure can vary substantially for cores that start from identical mass but different compositions or from identical composition but different masses. The plane is broadly separated into two key regions separated by a diagonal line stretching from roughly $M_{CO} \approx 2.5\,M_\odot$ and $X_C \approx 0.10$ to about $M_{CO} \approx 10\,M_\odot$ and $X_C \approx 0.4$, above (below) which carbon burns convectively (radiatively) in the centre. Most of the cores with convective central carbon-burning die compact with smaller M_{Fe}, M_4, and $\xi_{2.5}$, but the opposite is true for those with radiative central carbon burning. However, in agreement with prior studies, the final structure varies highly non-monotonically, with compact final cores forming beneath the diagonal line and extended final cores above it.

(iii) Applying a sample explosion criterion, we find that the final fates of these cores closely correlate with the pre-supernova structure (Fig. 3). Most stars which form smaller M_{Fe}, M_4, and $\xi_{2.5}$ end up exploding, and vice versa. Though the outcomes are strongly delineated by the central carbon-burning transition, there are substantial non-monotonic variations. Based on the distribution of three parameters and the associated outcomes from the adopted explosion criterion, we find the values that separate most of the explosions from most of the implosions to be $M_{Fe} = 1.54\,M_\odot$, $M_4 = 1.66\,M_\odot$, and $\xi_{2.5} = 0.18$ (Fig. 3 and Table 2).

(iv) We test the CO-core model results by recreating a subset of our grid through an independent open source stellar evolution code MESA. Though there are slight differences due to input setup, there is good overall agreement (Figs 4 and 5). We have also compared our calculations with red supergiant and helium star models embedding equivalent CO cores (Fig. 6). While the variations are in good agreement, especially for the helium stars and the lighter hydrogenic stars, there are substantial differences that point to the limitations of our approach. Our models are not perfect substitutes for the embedded CO cores of full stars, and they should only be applied to infer bulk trends in populations rather than individual models.

(v) Our results are easy to use. A table listing M_{Fe}, M_4, μ_4, and $\xi_{2.5}$ values, as well as the full pre-supernova structure and composition for each model are available for download (see Section 8 for details). A sample explosion criterion is discussed in Section 3.2, but we leave it up to the reader to explore other options. The initial conditions of the CO cores, X_C, and M_{CO}, can be easily extracted in population synthesis calculations that employ active or passive stellar evolution, and our results can be utilized as fast lookup tables. In Section 5.1, we demonstrate a sample application on a recent study on Type-IIb supernova progenitors. Though our results cannot be applied directly to rapid BPS calculations, in Section 5.2, we provide fitting functions for a simple estimate of X_C based on the CO-core mass.

Our future work will expand on a number of fronts. A followup study will be focused on the late stage evolution of CO cores, and will explore ways to model them to even more closely mimic embedded counterparts. We are also planning to develop a prescription for BPS codes to estimate the initial carbon mass fraction, X_C. The explodability of these cores will be explored in the context of the neutrino-driven mechanism and nucleosynthesis as well.

REFERENCES

Arnett W. D., 1972a, ApJ, 173, 393
Arnett W. D., 1972b, ApJ, 176, 681
Barkat Z., Marom A., 1990, in Wheeler J. C., Piran T., Weinberg S., eds, Supernovae, Jerusalem Winter School for Theoretical Physics. World Scientific Publishing Co., Singapore, p. 95
Barkat Z., Rakavy G., Sack N., 1967, Phys. Rev. Lett., 18, 379
Belczynski K., Bulik T., Kluźniak W., 2002b, ApJ, 567, L63
Belczynski K., Kalogera V., Bulik T., 2002a, ApJ, 572, 407
Belczynski K., Repetto S., Holz D. E., O'Shaughnessy R., Bulik T., Berti E., Fryer C., Dominik M., 2016, ApJ, 819, 108
Bennett M. E. et al., 2012, MNRAS, 420, 3047
Breivik K. et al., 2019, ApJ, 898, 71
Buchmann L., 1996, ApJ, 468, L127
Burrows A., Hayes J., Fryxell B. A., 1995, ApJ, 450, 830
Burrows A., Radice D., Vartanyan D., Aaron Skinner M., Dolence J. C., 2020, MNRAS, 491, 2715
Chieffi A., Limongi M., 2020, ApJ, 890, 43
Chrimes A. A., Stanway E. R., Eldridge J. J., 2020, MNRAS, 491, 3479
Couch S. M., Warren M. L., O'Connor E. P., 2020, ApJ, 890, 127
De Donder E., Vanbeveren D., 2004, New Astron. Rev., 48, 861
de Mink S. E., Sana H., Langer N., Izzard R. G., Schneider F. R. N., 2014, ApJ, 782, 7
Ebinger K., Curtis S., Fröhlich C., Hempel M., Perego A., 2019, ApJ, 870, 1
Eldridge J. J., Stanway E. R., 2016, MNRAS, 462, 3302
Eldridge J. J., Tout C. A., 2004, MNRAS, 353, 87
Eldridge J. J., Izzard R. G., Tout C. A., 2008, MNRAS, 384, 1109
Eldridge J. J., Stanway E. R., Xiao L., McClelland L. A. S., Taylor G., Ng M., Greis S. M. L., Bray J. C., 2017, PASA, 34, e058
Ertl T. et al., 2016, ApJ, 818, 124
Ertl T., Woosley S. E., Sukhbold T., Janka H. T., 2020, ApJ, 890, 51
Evans F. A., Renzo M., Rossi E. M., 2020, MNRAS, 497, 5344
Farmer R., Fields C. E., Petermann I., Dessart L., Cantiello M., Paxton B., Timmes F. X., 2016, ApJS, 227, 22
Fields C. E., Couch S. M., 2020, ApJ, 901, 33
Fraley G. S., 1968, Ap&SS, 2, 96
Fraser M. et al., 2013, ApJ, 779, L8
Fryer C. L., 1999, ApJ, 522, 413
Fryer C. L., Belczynski K., Wiktorowicz G., Dominik M., Kalogera V., Holz D., 2012, ApJ, 749, 91

Fuller J., 2017, MNRAS, 470, 1642

Fuller J., Ma L., 2019, ApJ, 881, L1

Fuller J., Ro S., 2018, MNRAS, 476, 1853

Giacobbo N., Mapelli M., 2018, MNRAS, 480, 2011

Giacobbo N., Mapelli M., Spera M., 2018, MNRAS, 474, 2959

Heger A., Woosley S. E., Martínez-Pinedo G., Langanke K., 2001, ApJ, 560, 307

Heger A., Woosley S. E., Spruit H. C., 2005, ApJ, 626, 350

Horiuchi S., Nakamura K., Takiwaki T., Kotake K., Tanaka M., 2014, MNRAS, 445, L99

Hurley J. R., Pols O. R., Tout C. A., 2000, MNRAS, 315, 543

Hurley J. R., Tout C. A., Pols O. R., 2002, MNRAS, 329, 897

Izzard R. G., Tout C. A., Karakas A. I., Pols O. R., 2004, MNRAS, 350, 407

Izzard R. G., Dray L. M., Karakas A. I., Lugaro M., Tout C. A., 2006, A&A, 460, 565

Izzard R. G., Glebbeek E., Stancliffe R. J., Pols O. R., 2009, A&A, 508, 1359

Janka H.-T., Melson T., Summa A., 2016, Annu. Rev. Nucl. Part. Sci., 66, 341

Johnson S. A., Kochanek C. S., Adams S. M., 2018, MNRAS, 480, 1696

Jones S. et al., 2013, ApJ, 772, 150

Jones S., Röpke F. K., Pakmor R., Seitenzahl I. R., Ohlmann S. T., Edelmann P. V. F., 2016, A&A, 593, A72

Kochanek C. S. et al., 2017, MNRAS, 467, 3347

Kruckow M. U., Tauris T. M., Langer N., Kramer M., Izzard R. G., 2018, MNRAS, 481, 1908

Langer N. et al., 2020, A&A, 638, A39

Limongi M., Chieffi A., 2018, ApJS, 237, 13

Mabanta Q. A., Murphy J. W., Dolence J. C., 2019, ApJ, 887, 43

Marchant P., Renzo M., Farmer R., Pappas K. M. W., Taam R. E., de Mink S. E., Kalogera V., 2019, ApJ, 882, 36

Mauerhan J. C. et al., 2013, MNRAS, 430, 1801

Mazurek T. J., 1982, ApJ, 259, L13

Meakin C. A., Arnett D., 2006, ApJ, 637, L53

Meakin C. A., Arnett D., 2007, ApJ, 667, 448

Melson T., Janka H.-T., Marek A., 2015, ApJ, 801, L24

Menon A., Heger A., 2017, MNRAS, 469, 4649

Müller B., Heger A., Liptai D., Cameron J. B., 2016, MNRAS, 460, 742

Nomoto K., Hashimoto M., 1988, Phys. Rep., 163, 13

Ohio Supercomputer Center 1987. Available at: http://osc.edu/ark:/19495/f5s1ph73

O'Connor E., Ott C. D., 2011, ApJ, 730, 70

O'Connor E. et al., 2018, J. Phys. G Nucl. Phys., 45, 104001

Pastorello A. et al., 2007, Nature, 447, 829

Patton, R. A, Sukhbold, T. 2020, Towards a Realistic Explosion Landscape for Binary Population Synthesis Zenodo, available at https://zenodo.org/record/3839747#.X4lVedAzbIU

Paxton B. et al., 2010, Astrophysics Source Code Library, record ascl:1010.083

Paxton B., Bildsten L., Dotter A., Herwig F., Lesaffre P., Timmes F., 2011, ApJS, 192, 3

Paxton B. et al., 2013, ApJS, 208, 4

Paxton B. et al., 2019, ApJS, 243, 10

Pejcha O., Thompson T. A., 2015, ApJ, 801, 90

Podsiadlowski P., Morris T. S., Ivanova N., 2007, Supernova 1987A: 20 Years After: Supernovae and Gamma-ray Bursters. AIP, USA, p. 125

Poelarends A. J. T., Wurtz S., Tarka J., Cole Adams L., Hills S. T., 2017, ApJ, 850, 197

Renzo M., Ott C. D., Shore S. N., de Mink S. E., 2017, A&A, 603, A118

Renzo M. et al., 2019, A&A, 624, A66

Sana H. et al., 2012, Science, 337, 444

Sana H. et al., 2013, A&A, 550, A107

Schneider F. R. N., Podsiadlowski P., Müller B., 2020, preprint (arXiv:2008.08599)

Shiode J. H., Quataert E., 2014, ApJ, 780, 96

Siess L., Izzard R. G., Davis P. J., Deschamps R., 2013, A&A, 550, A100

Spera M., Mapelli M., 2017, MNRAS, 470, 4739

Spera M., Mapelli M., Bressan A., 2015, MNRAS, 451, 4086

Spera M., Mapelli M., Giacobbo N., Trani A. A., Bressan A., Costa G., 2019, MNRAS, 485, 889

Sravan N., Marchant P., Kalogera V., 2019, ApJ, 885, 130

Stevenson S., Berry C. P. L., Mandel I., 2017b, MNRAS, 471, 2801

Stevenson S., Vigna-Gómez A., Mandel I., Barrett J. W., Neijssel C. J., Perkins D., de Mink S. E., 2017a, Nat. Commun., 8, 14906

Sukhbold T., Adams S., 2020, MNRAS, 492, 2578

Sukhbold T., Woosley S. E., 2014, ApJ, 783, 10

Sukhbold T., Ertl T., Woosley S. E., Brown J. M., Janka H.-T., 2016, ApJ, 821, 38

Sukhbold T., Woosley S. E., Heger A., 2018, ApJ, 860, 93

Ugliano M., Janka H.-T., Marek A., Arcones A., 2012, ApJ, 757, 69

Vartanyan D., Burrows A., Radice D., Aaron Skinner M., Dolence J., 2018, MNRAS, 477, 3091

Viallet M., Meakin C., Arnett D., Mocák M., 2013, ApJ, 769, 1

Vigna-Gómez A. et al., 2018, MNRAS, 481, 4009

Weaver T. A., Zimmerman G. B., Woosley S. E., 1978, ApJ, 225, 1021

Woosley S., Sukhbold T., Janka H.-T., 2020, ApJ, 896, 56

Woosley S. E., 2017, ApJ, 836, 244

Woosley S. E., 2019, ApJ, 878, 49

Woosley S. E., Heger A., 2015, ApJ, 810, 34

Woosley S. E., Weaver T. A., 1995, ApJS, 101, 181

Woosley S. E., Heger A., Weaver T. A., 2002, Rev. Mod. Phys., 74, 1015

Yadav N., Müller B., Janka H. T., Melson T., Heger A., 2020, ApJ, 890, 94

Yoon S.-C., Woosley S. E., Langer N., 2010, ApJ, 725, 940

Zapartas E. et al., 2017, A&A, 601, A29

Zapartas E. et al., 2019, A&A, 631, A5

This paper has been typeset from a TEX/LATEX file prepared by the author.